Int j simul model 23 (2024) 3, 447-458
Original scientific paper

DESIGN OF A PERIODIC STRUCTURE FOR COMPOSITE HELICOPTER ROTOR BLADE

Özel, M. A.[*,**] & Kopmaz, O.[*]
[*] Bursa Uludag University, Faculty of Engineering, Department of Mechanical Engineering, Görükle Kampusu, 16059 Nilüfer/Bursa, Turkey
[**] Oxodes, Görükle Mah. Üniversite-1 Cad. Ulutek Teknoloji Geliştirme Binası, 16059 Nilüfer/Bursa, Turkey
E-Mail: mertaliozel@uludag.edu.tr, okopmaz@uludag.edu.tr

Abstract
This study investigates the design and optimization of a 3D periodic structure to minimize vibrations in helicopter rotor blade systems. The research focuses on nonlinear models for rotating beams using a hybrid formulation of finite element methods and variational asymptotic beam sectional analysis. The periodic structure attenuates vibration transmitted from the blades to the rotor shaft. Dimension optimization was performed using particle swarm and gradient search algorithms, showing a minimal average difference of 2.37 %. Performance simulations at 190 rpm revealed that a 5.4 % reduction in reaction forces in the X and Y directions and a 3.2 % reduction in Z direction forces of main rotor shaft occur in comparison with conventional damper system. As a result of the study, it was concluded that 3D periodic structures can form a suitable passive damping system and mass reduction solution for helicopter blades.
(Received in June 2024, accepted in July 2024. This paper was with the authors 2 weeks for 1 revision.)

Key Words: 3D Periodic Structure, Composite Helicopter Rotor Blade, Vibration Attenuation, Passive Vibration Damping, Particle Swarm Optimization

1. INTRODUCTION

Rotor blade models are utilized in the design and analysis of engineering systems such as helicopters, turbines, and other airfoil structures [1, 2]. Accurate modelling and analysis of these systems are crucial for effectively ensuring aerodynamic performance, structural integrity, and vibration control [3]. Main problem of the rotary wing system is vibration. In a helicopter, there are three main sources of vibration: the rotor blade system, the engine, and the fuselage [3, 4]. Especially, a significant portion of vibration in the rotor blade system and fuselage is aerodynamically induced [5]. Various approaches exist to minimize vibration in rotor blade systems, categorized as active, semi-active, and passive vibration control systems [6-8]. Active systems can provide precise control by responding to varying disturbing vibration sources [9-11]. Similar performance can be achieved from semi-active systems [12]. However, the significant drawback of such systems lies in the challenge of positioning them on rotating structures [13, 14]. The primary advantage of passive vibration attenuating systems is their independence from external power sources, making them simpler in structure. Consequently, they are easier to implement, especially in rotor blade systems [15, 16]. The literature presents various passive vibration attenuation structures, one of which is structures with a periodic arrangement [17-19]. Periodic structures transmit vibrations by attenuating from one end of the structure to the other, based on their specific arrangement, geometry, and material properties within certain frequency ranges [19, 20]. The primary disadvantage of passive vibration attenuating systems is their limited response to varying vibration sources [20]. Hence, during the design phase, they should be tailored to achieve optimum performance under specified constraints using optimization methods. Zhang et al. [21], introduces a novel variable cross-section periodic structure support made of acrylonitrile-butadiene-styrene and investigates its band gap characteristics experimentally. The findings demonstrate that the variable cross-

section periodic structure effectively attenuates vibrations within the band gap frequency range compared to non-periodic structures. Arretche and Matlack [22], explores the impact of rotational speed on torsional band gaps in a rotating shaft with local resonances, considering stress stiffening effects. The findings indicate that the resonant frequency of beam-tip-mass resonators and the band gaps of acoustic metamaterials depend linearly on rotational speed, leading to effective vibration attenuation over a broad frequency range.

Mathematical models specific to the system are employed in the design of passive structures, necessitating a mathematical model simulating the rotor blade system. The Euler-Bernoulli beam theory is widely used in this models [23, 24]. It assumes that the cross-section of the beam remains perpendicular to the beam axis and has no warping. Furthermore, this theory allows considers the beam to be homogeneous and allows one to model deformation modes such as extension, torsion, and bending in two different directions. On the other hand, Timoshenko beam theory is used for beams where shear effects are taken into account [25]. The Timoshenko model is significant for composite beams, encompassing all deformation modes. For nonlinear problems, a modelling and analysis tool was developed named Variational Asymptotic Beam Sectional Analysis, VABS [26-29]. The VABS calculates structural and inertial properties of cross-sections through the finite element mesh of the geometry. The overall behaviour of one-dimensional beam analysis is achieved by investigating the three-dimensional point displacement and stress distribution within the structure.

The innovation introduced by this study encompasses the design of a periodic passive vibration attenuation structure for helicopter blades. The 2D composite cross-section of the helicopter blade has been discretized using finite element modelling. After, a 3D nonlinear dynamic model of the helicopter's rotor blade system was developed. Using the developed model, the dimension optimization of the periodic structure was conducted. Optimization was accomplished utilizing particle swarm and gradient approaches. The performance of the developed periodic structure was compared with that of a passive damper system. The characteristics of the damper system were calculated using the same optimization methods.

2. MATERIALS AND METHODS

In this section, the focus will be on modelling a rotor blade system that includes a periodic structure. Initially, the 2D composite blade section will be defined using the VABS analysis. This method will be applied to establish the composite material definitions for the skin, spar, and honeycomb regions of the blade section. Specifically, the skin and spar will be modelled as a composite laminate and the honeycomb as an orthotropic material. These definitions are essential for capturing the anisotropic behaviour of composite materials. Using the VABS algorithm, key structural properties such as the stiffness matrix, which characterizes the relationship between forces and deformations; the mass matrix, which describes the distribution of mass; the centre of mass; the shear centre, which is the point where shear forces do not cause twisting; and the neutral axis, which is the axis of zero bending stress, will be calculated. Subsequently, the analysis will be extended to three dimensions by constructing a 3D model of the blade. This will be done in the SIMSCAPE environment within the MATLAB/SIMULINK program, a platform that allows for the modelling and simulation of physical systems. The 3D model will incorporate the detailed 2D cross-sectional properties obtained from the VABS analysis. Hinged boundary conditions will be considered. Finally, a finite element method FEM will be performed using ANSYS, a widely used engineering simulation software. FEM will allow for the comparison of the results of the VABS and multibody analyses by providing a detailed stress and deformation distribution under various loading conditions. This comprehensive approach ensures that the results are robust and reliable, providing a thorough

understanding of the rotor blade system's behaviour. The schematic of the algorithm is shared in Fig. 1.

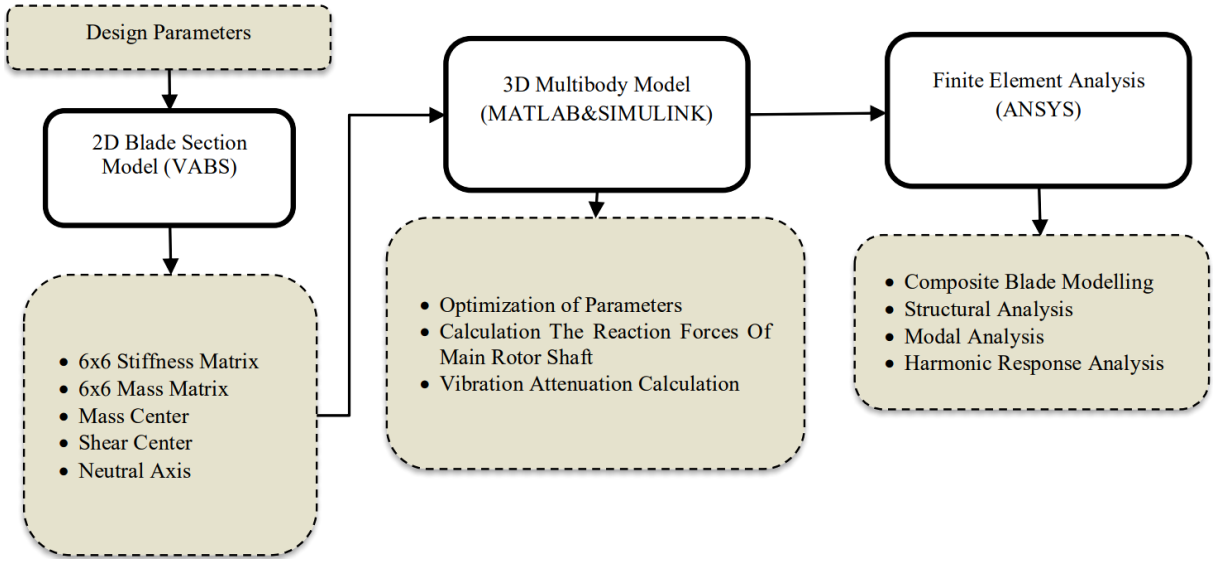


Figure 1: Algorithm of the mathematical modelling.

The 2D blade section defined within the VABS algorithm is shown in Fig. 2. The outermost region of the blade section, known as the skin, will be made of carbon fibre composite material, while the spar will be manufactured from glass fibre materials. The part extending towards the trailing edge contains honeycomb and glass fibre materials. The PreVABS algorithm, found within the VABS solver, has been utilized for this model.

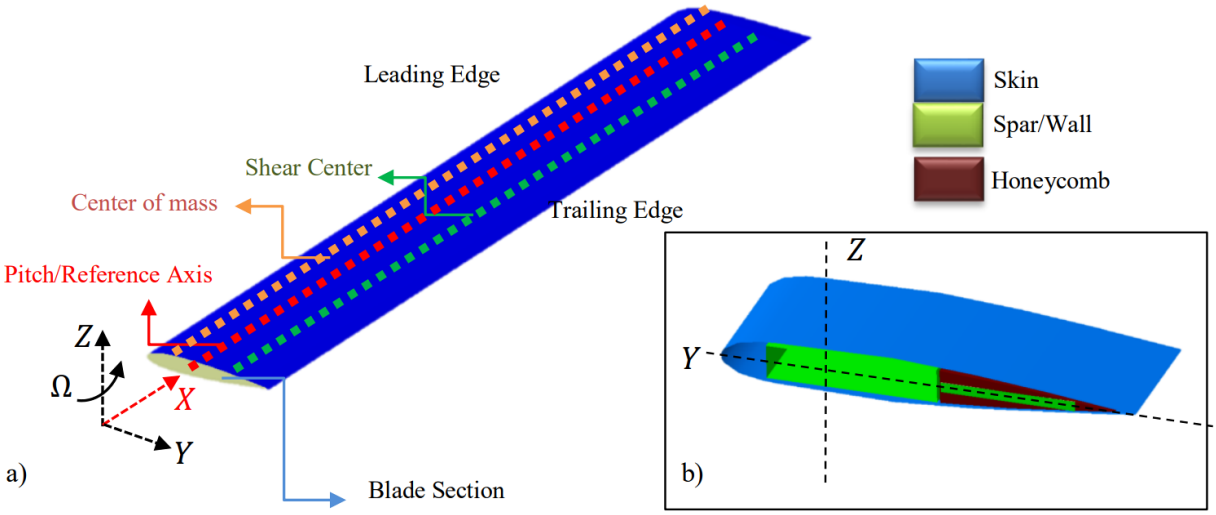


Figure 2: Composite blade; a) VABS model and b) blade section.

The parameters calculated in the VABS algorithm have been transferred to the MATLAB/SIMULINK software considering the FEM of the geometry. The FEM of the blade describes a flexible body as a superposition of a rigid-body model and a deformation model. The rigid-body model includes rotation and translation movements of the body without any deformation. The model calculates shape changes at specific points on the body. These shape changes are obtained using the rigid-body model incorporating the FEM. Obtaining accurate results from this method depends on the spatial distribution of the mass, inertia, stiffness, and damping properties of the geometry.

The FEM divides the body into a mesh with numerous corner points or nodes, each having six degrees of freedom. The mesh is determined by the motion equation shared in Eq. (1) respect to undamped situation.

$$\left(-\omega^2 \underset{\sim}{M} + \underset{\sim}{K}\right) \underset{\sim}{u_n} = \underset{\sim}{F} \tag{1}$$

Here, ω frequency, $\underset{\sim}{M}$ mass matrix**,** $\underset{\sim}{K}$ stiffness matrix**,** the vector $\underset{\sim}{u_n}$ represents the nodal movements of the nodes within the mesh structure. The matrix $\underset{\sim}{F}$ represents the external loads. Eqs. (2) and (3) are used for the state-space solution of the system.

$$\dot{\mathrm{x}}_{\underset{\sim}{S}} = \underset{\sim}{A}\, \underset{\sim}{x_S} + \underset{\sim}{B}\, \underset{\sim}{u_S} \tag{2}$$

$$\mathrm{y}_{\underset{\sim}{S}} = \underset{\sim}{C}\, \underset{\sim}{x_S} + \underset{\sim}{D}\, \underset{\sim}{u_S} \tag{3}$$

where, $\underset{\sim}{x_S}$, $\underset{\sim}{u_S}$ and $\mathrm{y}_{\underset{\sim}{S}}$ respectively denote the state, input, and output vectors. $\underset{\sim}{A}$, $\underset{\sim}{B}$, $\underset{\sim}{C}$, and $\underset{\sim}{D}$ represent the state, input, output, and state matrices. These matrices are computed from the mass and stiffness matrices obtained from a reduced FEM. For a rapid solution of the multi-degree-of-freedom model, the model needs to be reduced. Generally, nodes corresponding to high-frequency and low-deformation are eliminated in the model reduction process. Therefore, the obtained model generally conforms to the boundary conditions of the body. These nodes are called boundary nodes and they are connected to the axes of the final model accordingly. It is recommended that there be at least three axes for proper simulation of deformation. This study focuses on a model reduction method presented by Craig and Bampton [30]. This method is commonly used in the analysis of multiple body problems. A model reduction method reduces the complexity and the size of a model. The Craig-Bampton method achieves this reduction by neglecting all fixed-boundary vibration modes with frequencies above a certain threshold frequency. Ultimately, a simplified model with fewer variables is obtained depicted in Eq. (4).

$$\underset{\sim}{H} = [\tau_c \quad \tau_s] \tag{4}$$

Here, H is the Craig-Bampton transformation matrix, τ_c represents a set of constraints, and τ_s represents a set of fixed boundary mode shapes. Modes containing low deformation below the specified threshold frequency are reduced using $\underset{\sim}{H}$. The terms $\underset{\sim}{\overline{M_*}}$ include the reduced mass matrix $\underset{\sim}{\bar{M}}$ and the terms $\underset{\sim}{\overline{K_*}}$ include the reduced stiffness matrix $\underset{\sim}{\bar{K}}$.

$$\underset{\sim}{\overline{M_*}} = \underset{\sim}{H^T}\, \underset{\sim}{\bar{M}}\, \underset{\sim}{H} \tag{5}$$

$$\underset{\sim}{\overline{K_*}} = \underset{\sim}{H^T}\, \underset{\sim}{\bar{K}}\, \underset{\sim}{H} \tag{6}$$

Unit cells are defined as the smallest repeating unit within a periodic structure that can replicate in one, two, or three dimensions. The behaviour of an infinitely periodic structure can be anticipated by applying Floquet Bloch theory [31] to a single unit cell. This approach allows for the determination of the periodic structure, which describes the relationship between the wave vector and its frequency. Bloch's theorem characterizes waves in periodic materials. According to Bloch's theorem, the wave function of a particle in a periodically repeating structure can be represented in terms of the displacements of neighbouring unit cells as shown in Eq. (7).

$$u^{(n+j)} = e^{i\gamma d j} u^n \tag{7}$$

Here, u^n and $u^{(n+j)}$ represent the displacements of the n^{th} and $(n+j)^{\text{th}}$ masses, respectively, d is the distance between two adjacent particles, i is the imaginary unit and γ is the wave number. An infinite 1D periodic series are shown in Fig. 3 a. In 3D dimension, implementing Bloch's theorem can be challenging because degrees of freedom DOFs are present not only at the boundaries and corners but also on the surfaces, all of which must be taken into account.

The corresponding DOFs, marked with the same colours, are shown in Fig. 3 b [31]. These DOFs with the same colours are interconnected using Bloch boundary conditions. In helicopter blades, there are three significant motions that influence forced vibrations: torsion, lead-lag, and flap motions. The extension motion can be neglected because its effect is minimal when considering centrifugal stiffness. The most suitable periodic structure geometry is of the circular type under the influence of these motions as seen in Fig. 3 c. To correspond with the three motions occurring in three different axes, a unit cell composed of circles drawn on these three axes is used. This three-dimensional unit cell includes periodic connections with other cells as shown in Fig. 3 b. The boundary condition connections of each unit cell are also correlated with the VABS section model. The 3D Bloch periodicity matrix is depicted in Eq. (8).

$$\underset{\sim}{P} = \underset{\sim}{P_0} + \underset{\sim}{P_x}\,\lambda_x + \underset{\sim}{P_y}\,\lambda_y + \underset{\sim}{P_z}\,\lambda_z + \underset{\sim}{P_{xy}}\,\lambda_x\lambda_y + \underset{\sim}{P_{xz}}\,\lambda_x\lambda_z + \underset{\sim}{P_{yz}}\,\lambda_y\lambda_z + \underset{\sim}{P_{xyz}}\,\lambda_x\lambda_y\lambda_z \tag{8}$$

Here, $\underset{\sim}{P}$ is periodicity matrix and details are presented in [31]. $\lambda_m = e^{iγ_m a_m}$ and a_m is the translation vector component. The simplified model of the 3D Bloch periodicity matrix can be obtained using Eq. (4) likewise Eqs. (5) and (6).

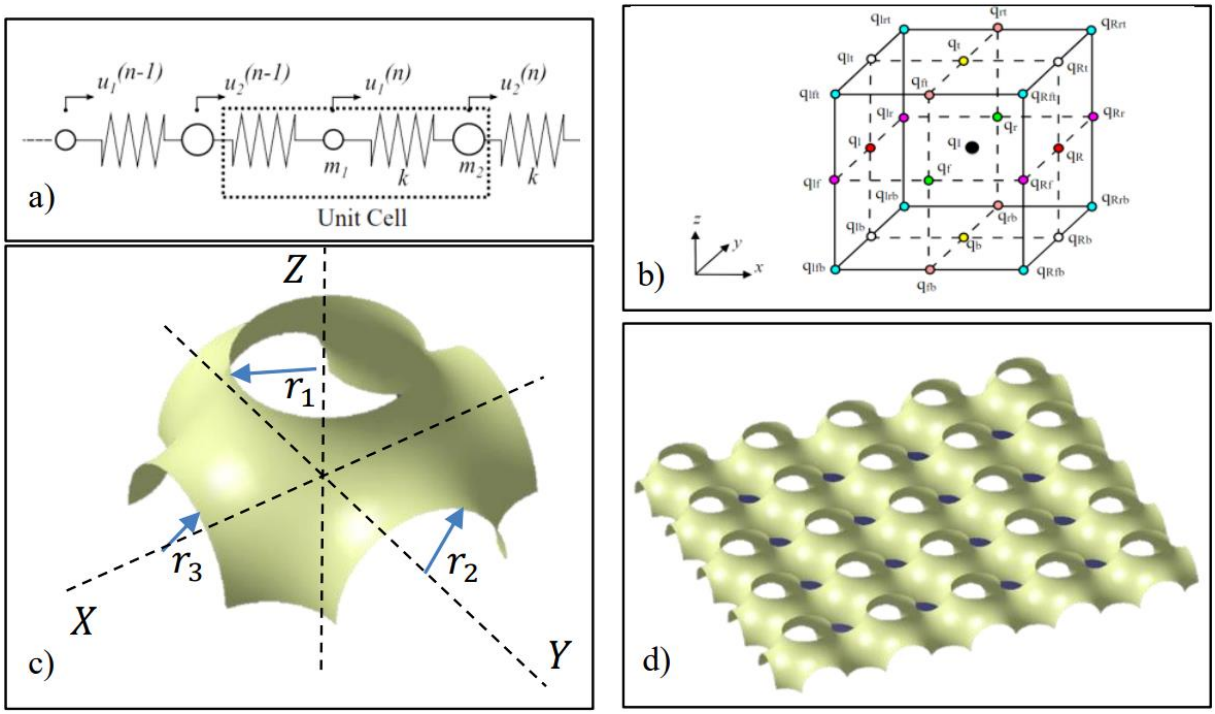


Figure 3: Periodic structure schematics; a) 1D periodic structure, b) 3D periodic unit cell [31], c) developed 3D unit cell geometry, d) periodic structure for helicopter blade.

This defined periodic geometry is positioned in the middle region of the spar/wall and honeycomb sections in the blade cross-section as shown in Fig. 4. In the spar/wall section, it is placed in a rectangular profile, and in the honeycomb section, it is positioned linearly along the blade direction. A FEM of the same structure will be performed using the ANSYS software to compare the MATLAB/SIMULINK results. The optimized geometry will first be defined as a composite structure. A modal analysis of the structure will be conducted under the same boundary conditions following the calculation of preload under working conditions. The harmonic behaviour of the structure will be examined using the mode superposition method. This will allow for the analysis of the band gap behaviour of the structure using the finite element method.

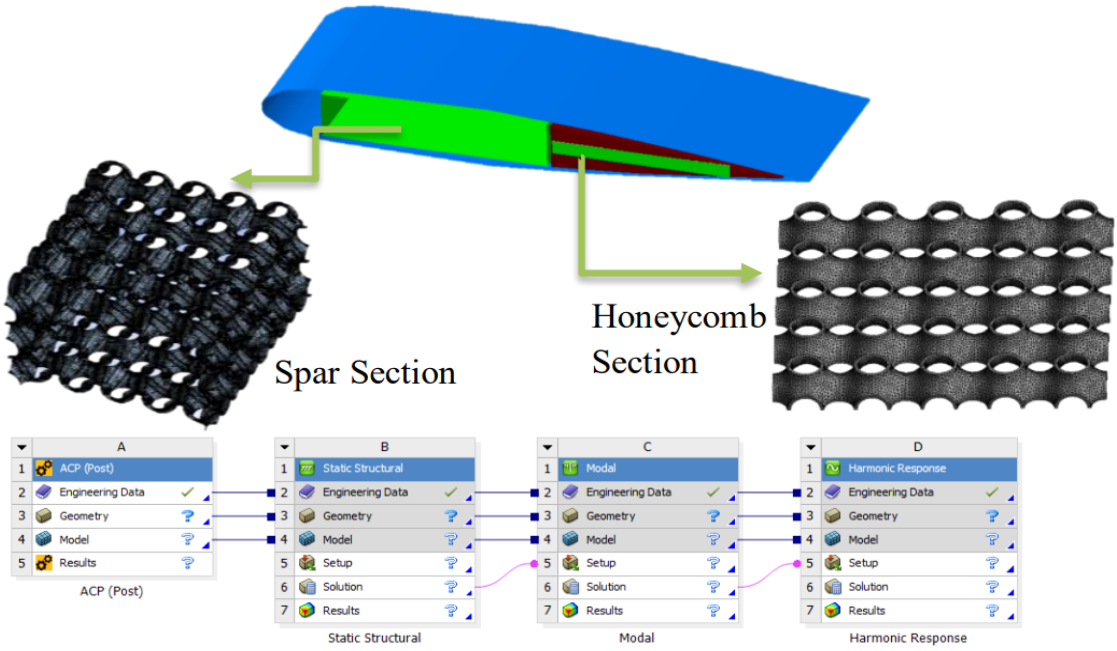


Figure 4: FEM model of the composite blade.

Dimension of the periodic structure is optimized using gradient search and particle swarm optimization. Cost function *CF* for the vibration attenuation is defined at below.

$$CF = \frac{Blade\ Root\ Acceleration\ (a_x, a_y, a_z, \alpha_x, \alpha_y, \alpha_z)}{Blade\ Tip\ Acceleration\ (a_x, a_y, a_z, \alpha_x, \alpha_y, \alpha_z)} \tag{9}$$

Here, a_x, a_y, a_z is linear accelerations and $\alpha_x, \alpha_y, \alpha_z$ angular accelerations for X, Y and Z direction respectively. The purpose of the cost function is to minimize the vibration transmissibility. The cost function is minimized with aid of a gradient descent algorithm. The gradient descent algorithm was selected because of its quick calculation time. The algorithm for n iterations for variable step size μ.

$$q_{k+1} = \hat{q}_k - \mu \frac{\nabla f}{||\nabla f||}, k = 0, 1, 2, \dots, n \tag{10}$$

$$\nabla f = J^T f(CF) \tag{11}$$

where, ∇f is error direction and J is Jacobian of the objective function. Also, the particle swarm optimization PSO method is used for comparing the results. Well-known PSO algorithm is depicted in [32]. The multibody model of the system has been created in the SIMSCAPE environment considering the VABS model and the periodic structure model, as shown in Fig. 5 a. In this setup, the vibrations occurring at the blade root and the main rotor shaft bearing will be analysed in a vacuum environment taking into account the control inputs from the swashplate mechanism. In the two-blade rotor system, swashplate movements will provide inputs to examine scenarios such as hovering and forward cruising. The rotor blade model that includes lead-lag, torsion, and flap dampers has also been created for comparing the results of the periodic structure, as shown in Fig. 5 b. The optimization algorithm introduced in Eq. (9) will also optimize these three damping parameters.

In the two-blade rotor system, dimensions of periodic structure including radius values of circles r_1, r_2, r_3 and thickness t are optimized. Also, damper coefficients (b_{lead}, b_{flap}, b_{tors}) are optimized for comparing the performance of the periodic structure. The design parameters are presented in Table I.

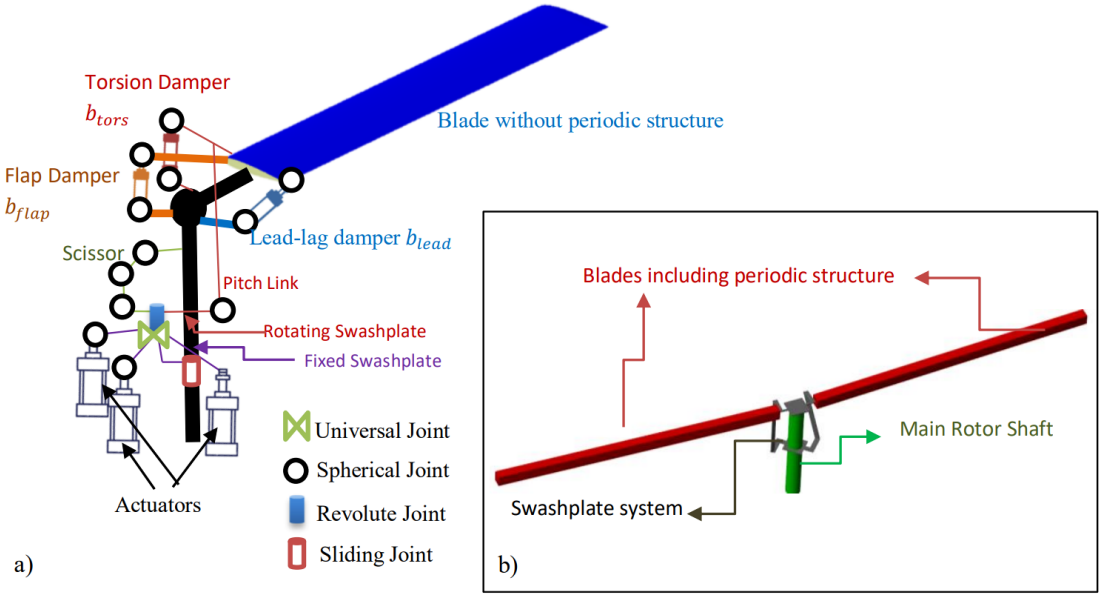


Figure 5: Multibody model of rotor blade system; a) damper system, b) periodic structure.

Table I: Design parameters.

Parameter	Lower bound	Upper Bound
r_1	10 mm	80 mm
r_2	10 m	80 mm
r_3	10 m	80 m
t	1 mm	15 mm
b_{lead}	0.5×10^5 N·s/m	5×10^5 N·s/m
b_{flap}	0.5×10^5 N·s/m	5×10^5 N·s/m
b_{tors}	0.5×10^5 N·s/m	5×10^5 N·s/m

The composite rotor blade system is developed based on the parameters depicted in Table II. The cross-section of the blade primarily comprises carbon fibre, glass fibre, honeycomb, film adhesives, and steel. The 0° lay-up angle aligns with the blade span axis. Carbon fibre lay-ups, configured as [+45/0/+45], are used for the skin. The spar/wall lay-up configurations are [+45/0/+45] using glass fibre. To prevent crushing in the trailing edge zone, honeycomb is utilized. Film adhesives including epoxy are applied between the lay-ups. A steel erosion shield is incorporated into the cross-section to protect against sand and dust abrasion. The nose block is made of 0° glass fibre material. The material properties are detailed in [33].

Table II: Properties of rotor blade system.

Parameter	Value	Unit
Number of blades	2	-
Rotor speed	190	rpm
Rotor radius/chord length	4/0.3	m
Airfoil profile	NACA0012	-
Main rotor shaft radius	0.075	m
Main rotor shaft young	70	GPa

3. RESULTS

In this section, size optimization for the periodic structure and damping coefficient optimization for the system were carried out using Gradient Search and PSO algorithms. According to the

results presented in Table III, there is an average difference of 2.37 % between the values. The value of radius r_2 directly affects the flap movement along with thickness. Radius r_1 plays a role in torsion, while radius r_3 is involved in the attenuation of lead-lag vibrations.

Table III: Optimization results.

Parameter	Gradient Search	PSO
r_1	15.7 mm	16.07 m
r_2	24.7 m	24.1 m
r_3	15.4 mm	14.9 m
t	5.4 mm	5.3 mm
b_{lead}	4.02×10^5 N·s/m	3.95×10^5 N·s/m
b_{flap}	4.53×10^5 N·s/m	4.64×10^5 N·s/m
b_{tors}	3.85×10^5 N·s/m	3.78×10^5 N·s/m

The performance of the periodic structure in the frequency domain is presented in Fig. 6. The results of the optimal parameters obtained using gradient search and PSO algorithms in SIMULINK are shared. The calculation formula is: $Transmittance = 10 \times log_{10} CF$. Additionally, analysis results from ANSYS are provided to validate the findings. Based on the harmonic response, the blade tip is considered as the input and the blade root as the output. The logarithmic result of the output-to-input ratio indicates the vibration attenuation performance. It is observed that there is an average difference of 2.45 % between the gradient search and PSO algorithm results. Meanwhile, an average error of 8.27 % is found between the ANSYS and SIMULINK results. According to the results, the designed system exhibits a stop band at an angular speed of 190 rpm. The band gap region ranges between 175 rpm and 205 rpm approximately for Gradient Search results. It is observed that the optimization results generate a band gap within the operating speed range.

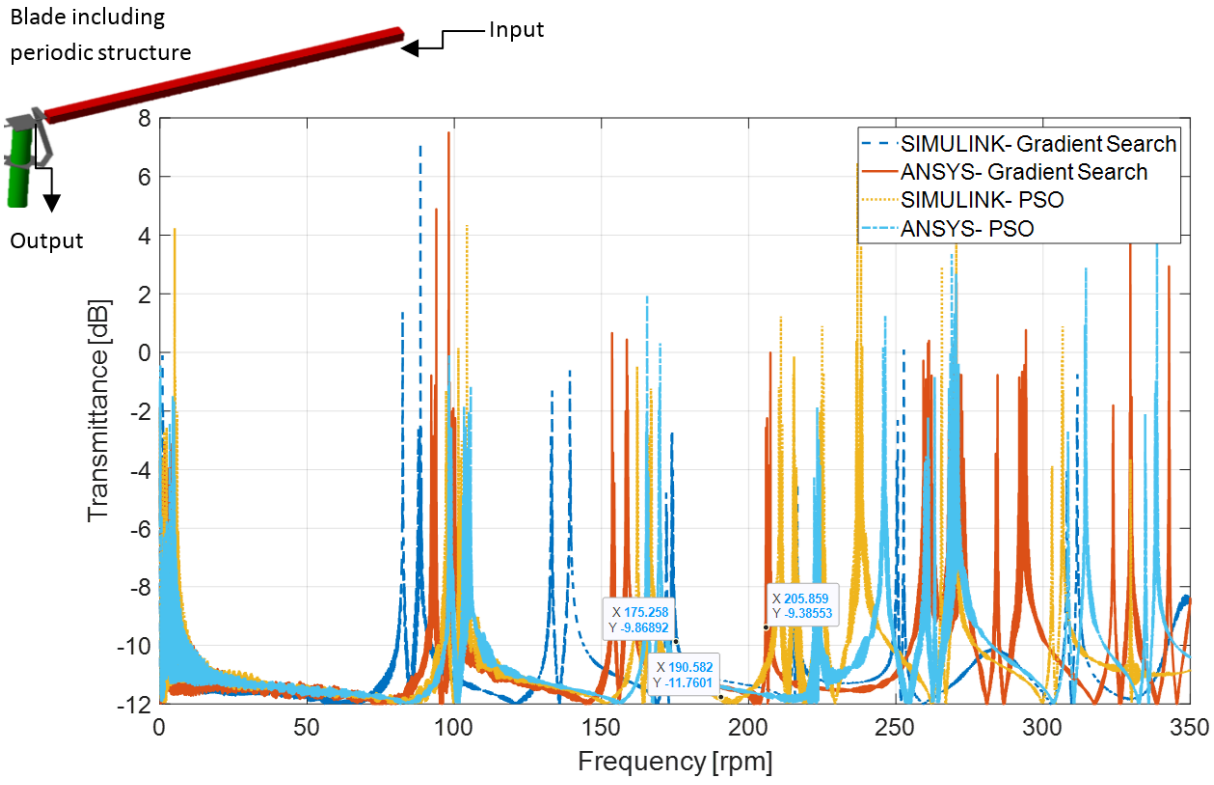


Figure 6: Band gap results respect to frequency.

Comparison of the periodic structure with the damper system will be made based on the reaction forces occurring at the bearing of the main rotor shaft. It is observed that the periodic structure reduces reaction forces by 5.4 % in the X and Y directions compared to the damper system at a constant angular speed of 190 rpm (linearly increased from 0 rpm to 190 rpm until 3 seconds) and 0° tilt angle. Additionally, the periodic structure demonstrates similar behaviour to the damper system by damping oscillatory forces to a certain extent in shown in Fig. 7.

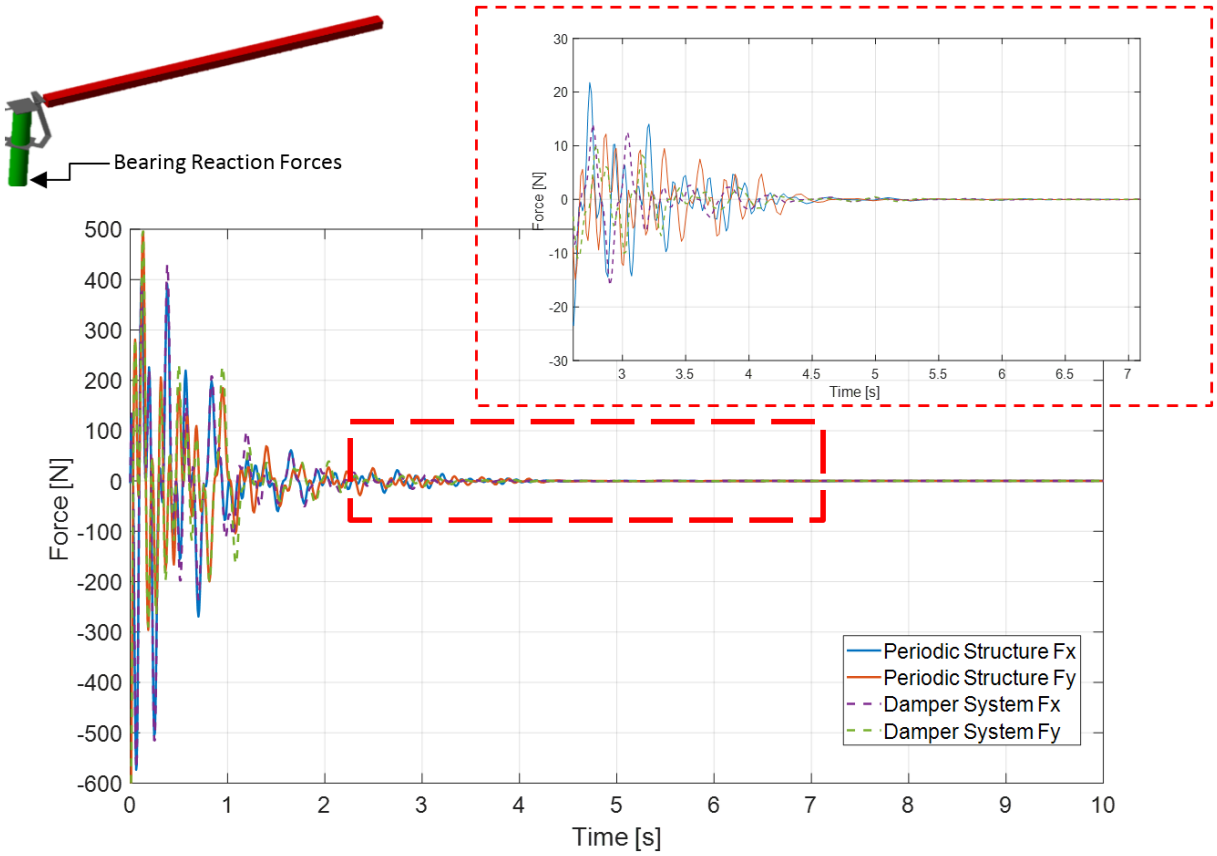


Figure 7: Bearing reaction forces comparison for periodic structure and damper system (Tilt angle 0°).

The effect of the reaction force in the Z direction with a tilt angle of 0 degrees is also shown in Fig. 8 a. It is observed that the periodic structure reduces this force, which is mainly caused by flap movement, by 3.2 %. A similar improvement is seen in the resultant accelerations at the centre of gravity of the main rotor shaft, where the periodic structure improves the acceleration values by 2.5 %.

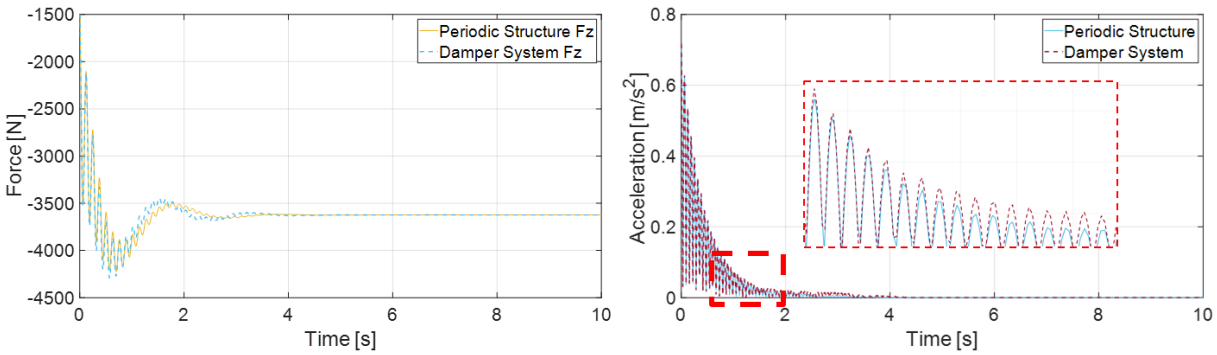


Figure 8: Bearing; a) reaction force at z direction, b) acceleration (Tilt angle 0°).

When the tilt angle is 10 degrees, the bearing forces and vibration values at the centre of gravity of the main rotor shaft increase due to the angular change. The periodic structure has shown an improvement of 1.5 % in reaction forces and 1.2 % in acceleration values in response to the changing tilt angle as shown in Fig. 9.

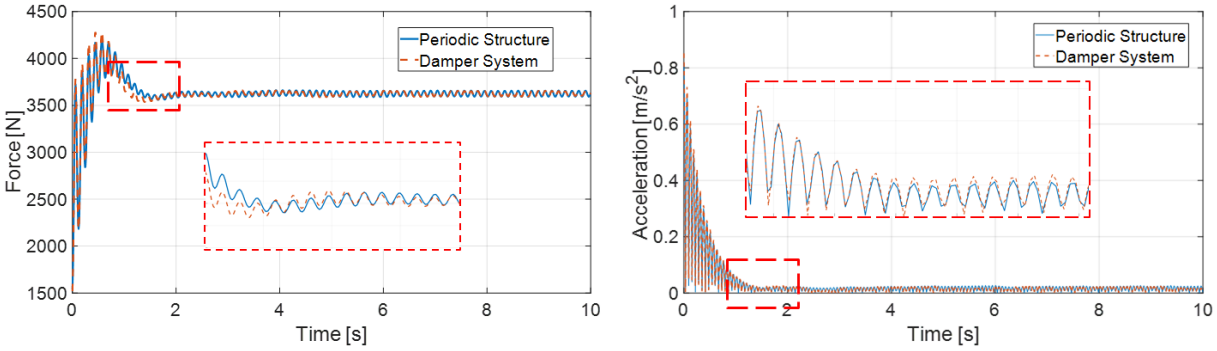


Figure 9: Bearing; a) reaction force (resultant), b) acceleration (Tilt angle 10°).

4. CONCLUSION

In this study, the design and optimization of a periodic structure are investigated for minimizing vibrations in the rotor blade system of helicopters. The equations of motion were derived using hybrid formulations combining the partial finite element approach and VABS, with a focus on nonlinear models for rotating beams. The model demonstrated that the periodic structure effectively minimizes the transmission of vibration from the helicopter blades to the main rotor shaft. This novel approach involves the design of a passive vibration attenuation system specifically for helicopter blades, showcasing the potential for significant improvements in vibration control. The dimension optimization of the periodic structure was conducted using PSO and gradient search algorithms, providing a robust framework for enhancing vibration performance. The optimization results, presented in Table III, indicated a minimal average difference of 2.37 % between the gradient search and PSO algorithm outcomes. The harmonic response analysis further validated the effectiveness of the periodic structure, as shown in Fig. 6, with an average error of 8.27 % between the ANSYS and SIMULINK results, confirming accuracy of the model. Performance analysis at a constant angular speed of 190 rpm with a 0° tilt angle demonstrated a 5.4 % reduction in reaction forces in the X and Y directions when using the periodic structure compared to a damper system. Additionally, the periodic structure exhibited similar damping behaviour to the damper system, effectively mitigating oscillatory forces. Further analysis during forward directional movement led to increased bearing forces and vibration values. Despite these increases, the periodic structure demonstrated an improvement of 1.5 % in reaction forces and 1.2 % in acceleration values under these conditions, indicating its robustness in various operational scenarios. Overall, the findings of this study underscore the effectiveness of the periodic structure in minimizing vibrations in helicopter rotor blade systems. The optimized design not only enhances vibration attenuation but also maintains performance across different operating conditions, providing a promising solution for improving the dynamic behaviour and basic system for helicopters. Within the scope of this study, it is clearly demonstrated that using passive periodic structure enables the production of a rotor system that is simpler and has fewer parts compared to traditional damper systems. The periodic structure possesses a geometry suitable for mass production thanks to appropriate mod shapes. In future work, the aim is to manufacture the periodic structure and validate it experimentally.

ACKNOWLEDGEMENT

Mert Ali Özel is a scholarship holder in TUBITAK 2244 – Industrial Ph.D. Fellowship Program. We would like to thank TUBITAK for their support. This study was developed within the scope of TUBITAK 118C100 project.

REFERENCES

[1] Sarker, P.; Chakravarty, U. K. (2021). On the dynamic response of a hingeless helicopter rotor blade, *Aerospace Science and Technology*, Vol. 115, Paper 106741, 23 pages, doi:10.1016/j.ast.2021.106741

[2] Lee, Y.-L.; Kim, D.-H.; Park, J.-S.; Hong, S.-B. (2020). Vibration reduction simulations of a lift-offset compound helicopter using two active control techniques, *Aerospace Science and Technology*, Vol. 106, Paper 106181, 15 pages, doi:10.1016/j.ast.2020.106181

[3] Vouros, S.; Polyzos, N. D.; Goulos, I.; Pachidis, V. (2021). Impact of optimized variable rotor speed and active blade twist control on helicopter blade–vortex interaction noise and environmental impact, *Journal of Fluids and Structures*, Vol. 104, Paper 103285, 22 pages, doi:10.1016/j.jfluidstructs.2021.103285

[4] Zhou, Q. H.; Qiu, Y. H.; Liu, H. S.; He, Y. (2023). A performance study on structural parameters of centre-axle-trailer combinations, *International Journal of Simulation Modelling*, Vol. 22, No. 1, 168-179, doi:10.2507/IJSIMM22-1-CO5

[5] Turan, M. K.; Erzan Topcu, E.; Karpat, F. (2024). Modelling and investigation of a driver seat suspension with negative stiffness structure, *International Journal of Simulation Modelling*, Vol. 23, No. 2, 275-286, doi:10.2507/IJSIMM23-2-684

[6] Jokar, H.; Vatankhah, R.; Mahzoon, M. (2023). Active vibration control of horizontal-axis wind turbine blades using disturbance observer-based boundary control approach, *Engineering Structures*, Vol. 275, Part B, Paper 115323, 14 pages, doi:10.1016/j.engstruct.2022.115323

[7] Meng, Z. S.; Peng, H. X.; Xie, Y. Y. (2023). Analysis of the dynamic load characteristics of double-top-beam supports with gaps, *International Journal of Simulation Modelling*, Vol. 22, No. 2, 291-302, doi:10.2507/IJSIMM22-2-650

[8] Koide, R. M.; Herrera, P. H.; Luersen, M. A.; Ferreira, A. P. C. S. (2024). Post-buckling optimisation of composite structures using a firefly algorithm, *International Journal of Simulation Modelling*, Vol. 23, No. 1, 5-16, doi:10.2507/IJSIMM23-1-654

[9] Ma, J.; Lu, Y.; Su, T.; Guan, S. (2021). Experimental research of active vibration and noise control of electrically controlled rotor, *Chinese Journal of Aeronautics*, Vol. 34, No. 11, 106-118, doi:10.1016/j.cja.2020.10.027

[10] Jayatilake, S.; Wu, J.; Titurus, B. (2023). Tendon-inerter-damper helicopter blade augmentation for improved dynamic performance, *Journal of Sound and Vibration*, Vol. 547, Paper 117509, 29 pages, doi:10.1016/j.jsv.2022.117509

[11] Bertolino, A. C.; Gaidano, M.; Smorto, S.; Porro, P. G.; Sorli, M. (2023). Development of a high-performance low-weight hydraulic damper for active vibration control of the main rotor on helicopters – Part 1: design and mathematical model, *Aerospace*, Vol. 10, No. 5, Paper 391, 20 pages, doi:10.3390/aerospace10050391

[12] Pulok, M. K. H.; Chakravarty, U. K. (2024). Aerodynamics and vibration analysis of a helicopter rotor blade, *Acta Mechanica*, Vol. 235, No. 5, 3033-3057, doi:10.1007/s00707-024-03871-9

[13] Yang, J.; Deng, J.; Zhao, J.; Jiao, S.; Long, X. (2024). A novel parallel multi-harmonic global multi-channel control algorithm for helicopter active vibration control, *Control Engineering Practice*, Vol. 142, Paper 105772, 20 pages, doi:10.1016/j.conengprac.2023.105772

[14] Shang, L.; Xia, P.; Zhang, J.; Lin, C. (2024). Geometrically exact aeroelastic stability analysis of helicopter composite rotor blades in forward flight, *Aerospace Science and Technology*, Vol. 144, Paper 108818, 15 pages, doi:10.1016/j.ast.2023.108818

[15] Machado, M. R.; Dutkiewicz, M. (2024). Wind turbine vibration management: an integrated analysis of existing solutions, products, and open-source developments, *Energy Reports*, Vol. 11, 3756-3791, doi:10.1016/j.egyr.2024.03.014

[16] Fink, A.; Schatz, R. (2023). Structurally integrated constrained layer damping for noise reduction on sandwich and semi-monocoque helicopter structures, *Composite Structures*, Vol. 322, Paper 117354, 16 pages, doi:10.1016/j.compstruct.2023.117354
[17] Wan, Z.; Zhu, X.; Li, T.; Han, Y.; Guo, W. (2023). A combined periodic acoustic black hole beams with wide vibration attenuation bands, *Thin-Walled Structures*, Vol. 193, Paper 111221, 9 pages, doi:10.1016/j.tws.2023.111221
[18] Wang, G.; Wan, S.; Hong, J.; Liu, S.; Li, X. (2023). Enhancement of the vibration attenuation characteristics in local resonance metamaterial beams: theory and experiment, *Mechanical Systems and Signal Processing*, Vol. 188, Paper 110036, 15 pages, doi:10.1016/j.ymssp.2022.110036
[19] Li, Y.; He, H.; Chen, H.; Liu, Y.; Wang, W.; Dong, J.; Jin, F.; Fan, H. (2023). Composite wave attenuation mechanism of periodic layered metastructure with embedded rubber-mass resonators, *Construction and Building Materials*, Vol. 384, Paper 131322, 8 pages, doi:10.1016/j.conbuildmat.2023.131322
[20] Patro, S. R.; Banerjee, A.; Ramana, G. V. (2023). Vibration attenuation characteristics of finite locally resonant meta beam: theory and experiments, *Engineering Structures*, Vol. 278, Paper 115506, 11 pages, doi:10.1016/j.engstruct.2022.115506
[21] Zhang, J.; Xia, X.; Wen, X.; Zang, M.; Dou, Y. (2022). Investigations on the band-gap characteristics of variable cross-section periodic structure support made of acrylonitrile-butadiene-styrene, *Materials*, Vol. 15, No. 12, Paper 4308, 17 pages, doi:10.3390/ma15124308
[22] Arretche, I.; Matlack, K. H. (2023). Centrifugal forces enable band gaps that self-adapt to synchronous vibrations in rotating elastic metamaterial, *Mechanical Systems and Signal Processing*, Vol. 202, Paper 110689, 15 pages, doi:10.1016/j.ymssp.2023.110689
[23] Mogehi, M. K.; Mohammadimehr, M.; Duc, N. D. (2024). Vibration analysis of a sandwich Timoshenko beam reinforced by GOAM/CNT with various boundary conditions using VIM, *Materials Science and Engineering: B*, Vol. 304, Paper 117364, 11 pages, doi:10.1016/j.mseb.2024.117364
[24] Seer, T. A.; Vahdati, N.; Shiryayev, O. (2019). Adaptive torsional tuned vibration absorber for rotary equipment, *Vibration*, Vol. 2, No. 2, 116-134, doi:10.3390/vibration2010008
[25] Moshir, S. K.; Hoa, S. V.; Shadmehri, F. (2024). Cross-sectional analysis of initially curved composite beams with rectangular and circular sections using an asymptotic meshless method, *International Journal of Solids and Structures*, Vol. 296, Paper 112827, 15 pages, doi:10.1016/j.ijsolstr.2024.112827
[26] Shakya, N. K.; Padhee, S. S. (2023). Asymptotic analysis of Timoshenko-like orthotropic beam with elliptical cross-section, *European Journal of Mechanics – A/Solids*, Vol. 102, Paper 105100, 13 pages, doi:10.1016/j.euromechsol.2023.105100
[27] Jie, Y.; Yifeng, Z.; Hui, Y.; Evrard, I. A. (2023). Dimension reduction model for sandwich panels with novel triangular chiral honeycomb using variational asymptotic method, *Thin-Walled Structures*, Vol. 193, Paper 111297, 20 pages, doi:10.1016/j.tws.2023.111297
[28] Tamer, A.; Zanoni, A.; Cocco, A.; Masarati, P. (2021). A generalized index for the assessment of helicopter pilot vibration exposure, *Vibration*, Vol. 4, No. 1, 133-150, doi:10.3390/vibration4010012
[29] Molina-Villegas, J. C.; Ballesteros Ortega, J. E.; Martínez Martínez, G. (2023). Closed-form solution for non-uniform Euler–Bernoulli beams and frames, *Engineering Structures*, Vol. 292, Paper 116381, 17 pages, doi:10.1016/j.engstruct.2023.116381
[30] Craig, R. R.; Bampton, M. C. C. (1968). Coupling of substructures for dynamic analyses, *AIAA Journal*, Vol. 6, No. 7, 1313-1319, doi:10.2514/3.4741
[31] Yao, L.; Jiang, G.; Wu, F.; Luo, J. (2019). Band structure computation of two-dimensional and three-dimensional phononic crystals using a finite element-least square point interpolation method, *Applied Mathematical Modelling*, Vol. 76, 591-606, doi:10.1016/j.apm.2019.05.052
[32] Wang, D.; Tan, D.; Liu, L. (2018). Particle swarm optimization algorithm: an overview, *Soft Computing*, Vol. 22, No. 2, 387-408, doi:10.1007/s00500-016-2474-6
[33] Visweswaraiah, S. B.; Ghiasi, H.; Pasini, D.; Lessard, L. (2013). Multi-objective optimization of a composite rotor blade cross-section, *Composite Structures*, Vol. 96, 75-81, doi:10.1016/j.compstruct.2012.09.031